Structural and Biochemical Studies on the Regulation of Biotin Carboxylase by Substrate Inhibition and Dimerization[*]

Chi-Yuan Chou[‡§] **and Liang Tong**[§1]

From the [‡]*Department of Life Sciences and Institute of Genome Sciences, National Yang-Ming University, Taipei 112, Taiwan and the* [§]*Department of Biological Sciences, Columbia University, New York, New York 10027*

Biotin carboxylase (BC) activity is shared among biotin-dependent carboxylases and catalyzes the Mg-ATP-dependent carboxylation of biotin using bicarbonate as the CO_2 donor. BC has been studied extensively over the years by structural, kinetic, and mutagenesis analyses. Here we report three new crystal structures of *Escherichia coli* BC at up to 1.9 Å resolution, complexed with different ligands. Two structures are wild-type BC in complex with two ADP molecules and two Ca^{2+} ions or two ADP molecules and one Mg^{2+} ion. One ADP molecule is in the position normally taken by the ATP substrate, whereas the other ADP molecule occupies the binding sites of bicarbonate and biotin. One Ca^{2+} ion and the Mg^{2+} ion are associated with the ADP molecule in the active site, and the other Ca^{2+} ion is coordinated by Glu-87, Glu-288, and Asn-290. Our kinetic studies confirm that ATP shows substrate inhibition and that this inhibition is competitive against bicarbonate. The third structure is on the R16E mutant in complex with bicarbonate and Mg-ADP. Arg-16 is located near the dimer interface. The R16E mutant has only a 2-fold loss in catalytic activity compared with the wild-type enzyme. Analytical ultracentrifugation experiments showed that the mutation significantly destabilized the dimer, although the presence of substrates can induce dimer formation. The binding modes of bicarbonate and Mg-ADP are essentially the same as those to the wild-type enzyme. However, the mutation greatly disrupted the dimer interface and caused a large re-organization of the dimer. The structures of these new complexes have implications for the catalysis by BC.

Escherichia coli biotin carboxylase (BC)[2] is one of the subunits of acetyl-CoA carboxylase (1–3) that belongs to the family of biotin-dependent carboxylases (4). The BC subunit catalyzes the first half-reaction, the Mg^{2+}-ATP-dependent carboxylation of biotin, which is covalently linked to biotin carboxyl carrier protein. Then carboxyltransferase activity transfers the carboxyl group from carboxybiotin to the acetyl-CoA acceptor (3, 5). In this family the carboxyltransferase components can differ greatly in sequence and structure, dependent on the identity of the acceptor molecule, such as acetyl-CoA, propionyl-CoA, methylcrotonyl-CoA, pyruvate, and urea (5–9). On the other hand, the BC components have significant amino acid sequence homology and show the same activity among all of these enzymes (2, 7–12).

The catalysis of BC has been studied extensively over the years by kinetic and mutagenesis analyses, and structural information is available for BC from many different organisms (2, 4, 13–21). The structure of BC contains three domains, A, B, and C domains, and the active site is located at the interface among the domains. The binding mode of the Mg-ADP, biotin, and bicarbonate substrates to BC, which was reported recently (22), offers significant insights into the catalytic mechanism of BC and greatly extends earlier studies with the ATP complexes of BC (16, 23).

Prokaryotic BC is a stable dimer with an extensive interface, and previous studies have suggested that dimerization may be required for the activity of this enzyme (24). This appears to be supported by the observations that the BC component of eukaryotic acetyl-CoA carboxylase is monomeric in solution and is catalytically inactive (14, 25). However, mutations in the dimer interface can greatly destabilize the dimer, and the resulting monomeric mutants are still catalytically active (26). A homologous BC dimer is observed in the structure of the holoenzyme of pyruvate carboxylase (7, 8, 27). In contrast, the BC component is monomeric in the $\alpha_6\beta_6$ holoenzyme of propionyl-CoA carboxylase (6). The mechanism of how dimerization can regulate the catalytic activity of prokaryotic BC is still not fully understood.

Here we report the crystal structures of wild-type *E. coli* BC in complex with two ADP molecules and two Ca^{2+} ions or in complex with two ADP molecules and one Mg^{2+} ion at 2.0 and 1.9 Å resolution. The second ADP molecule occupies the binding sites of bicarbonate and biotin, and our kinetic studies confirm substrate inhibition by ATP and demonstrate that this inhibition is competitive with respect to bicarbonate. Other nucleotides and pyrophosphate can also inhibit BC activity. To further characterize the effects of the dimer interface on BC catalysis, we have introduced another mutation, R16E, near the interface. The mutant has roughly half the catalytic activity compared with the wild-type enzyme. The K_d value (445 μM) for the mutant dimer is significantly higher than that for wild-type BC, although the presence of substrates can induce dimer formation. Our crystal structure revealed a dimeric form of this

mutant but with a significant re-organization of the dimer interface. The structure is also in complex with Mg-ADP and bicarbonate, offering another observation of the binding modes of these two substrates to BC.

MATERIALS AND METHODS

Crystals of wild-type *E. coli* BC in complex with two ADPs and two Ca^{2+} ions were obtained at room temperature by the sitting-drop vapor diffusion method. The protein solution was at 10 mg/ml concentration, which also included 5 mM Mg-AMPPNP, 44 mM biocytin, and 20 mM bicarbonate. The reservoir solution contained 17% (w/v) PEG3350 and 0.14 M $CaCl_2$. All crystals were cryo-protected in the reservoir solution supplemented with 12% (v/v) glycerol and flash-frozen in liquid nitrogen.

Crystals of wild-type *E. coli* BC in complex with two ADPs and one Mg^{2+} ion were obtained at room temperature by the sitting-drop vapor diffusion method. The protein solution was at 10 mg/ml concentration, which also included 10 mM Mg-ADP, 44 mM biocytin, and 20 mM bicarbonate. The reservoir solution contained 0.1 M Bis-tris (pH 6.2), 15% (w/v) PEG3350, 0.1 M NH_4Cl, and 5% (w/v) *n*-octyl-β-D-glucoside.

X-ray diffraction data were collected at 100 K at the National Synchrotron Light Source beamline X4A (x-ray wavelength 0.9795 Å). The diffraction images were processed and scaled with the HKL package (28). The crystal belongs to space group *C*2, with unit cell parameters of $a = 170.2$ Å, $b = 58.8$ Å, $c = 85.1$ Å, and $\beta = 94.2°$. There is a BC dimer in the asymmetric unit.

The structure was solved by the molecular replacement method with the program Phaser (29) using the structure of the wild-type BC with all substrates (PDB code 3G8C) as the search model (22). Manual rebuilding of the structure model was performed with O (30), and structure refinement was carried out with the programs CNS (31) and Refmac (32). The data processing and refinement statistics are summarized in Table 1. The crystal structures have been deposited at the Protein Data Bank (accession codes 3RUP, 3RV3, and 3RV4).

The R16E mutant of *E. coli* BC was produced with the QuikChange kit (Stratagene) and verified by DNA sequencing. The His tag on the recombinant enzyme was removed with thrombin during purification. The enzyme activity of the wild-type and mutant BC was determined spectrophotometrically at 340 nm at 30 °C following a published protocol (13). The reaction mixture contained 100 mM Hepes (pH 8.0), 15 mM sodium bicarbonate, 5 mM free $MgCl_2$, 40 mM biotin (from a 500 mM stock, with pH adjusted to 8.0), 0.2 mM NADH, 0.5 mM phosphoenolpyruvate, 7 units of lactate dehydrogenase (LDH), 4.2 units of pyruvate kinase (PK), and varying concentrations of Mg-ATP (from a 200 mM stock, dissolved in 100 mM Hepes (pH 8.0)). For the saturation pattern at low ATP concentrations, the Michaelis-Menten equation was used to fit the data. The non-hyperbolic pattern at higher ATP concentrations displayed substrate inhibition and, hence, was analyzed by the equation,

$$v = k_{cat}[E][S]/(K_m + [S] + [S]^2/K_i) \qquad \text{(Eq. 1)}$$

where k_{cat} is the catalytic constant, $[E]$ the enzyme concentration, $[S]$ the substrate concentration, K_m the apparent Michae-

lis constant of the Mg-ATP substrate, and K_i is the dissociation constant for the inhibitory enzyme-substrate complex (ES_2). The program SigmaPlot (Systat Software, Inc., Richmond, CA) was used for the data analysis.

To characterize the nature of the inhibition by ATP, kinetic assays were carried out with bicarbonate as the substrate (1–40 mM) and at varying concentrations of Mg-ATP (1.5–20 mM). For the inhibition assay with other compounds, various concentrations of Mg-GTP, Mg-CTP, and Mg-TTP were added into the reaction mixture with 0.2 mM Mg-ATP. Relative activities were used to measure the inhibition.

To confirm that the observed substrate inhibition by ATP was truly due to an effect on BC rather than the coupling enzymes (PK/LDH), assays were carried out with the coupling enzymes only in the presence of 0.1 mM ADP and 1, 5, 10, and 20 mM Mg-ATP, respectively. The results indicated that Mg-ATP did not have a significant effect on PK/LDH, which would not produce an apparent inhibition of the BC reaction in our assays. Similarly, Mg-GTP and magnesium pyrophosphate did not have a significant effect on the coupling enzymes either.

Crystals of the R16E mutant in complex with bicarbonate and Mg-ADP were obtained in the presence of 5 mM Mg-ATP, 44 mM biocytin, and 20 mM bicarbonate with 10 mg/ml protein. The reservoir solution contained 18% (w/v) PEG3350, 0.17 M CsCl, and 4% (v/v) methanol. X-ray diffraction data were collected at the NE-CAT beamline at the Advanced Photon Source. The structure was solved and refined followed the protocol described above for the wild-type enzyme. The crystal belongs to space group *C*2, with unit cell parameters of $a = 119.4$ Å, $b = 51.2$ Å, $c = 84.2$ Å, and $\beta = 119.8°$. There is a monomer of the R16E mutant in the asymmetric unit. The detailed crystallographic statistics are summarized in Table 1.

Analytical ultracentrifugation (AUC) experiments on the R16E mutant were performed on an XL-A analytical ultracentrifuge (Beckman, Fullerton, CA) with an An-50 Ti rotor (33). The R16E mutant at three different concentrations (1, 4, and 20 μM) with 100 mM Hepes (pH 8.0) was used to estimate the dynamic monomer-dimer content. The sample (330 μl) and reference (370 μl) solutions were loaded into a double-sector *epon* charcoal-filled centerpiece and centrifuged at 20 °C with a rotor speed of 42,000 rpm. Absorbance at 280 nm was monitored in a continuous mode with a time interval of 480 s and a step size of 0.003 cm. Multiple scans at different time intervals at three protein concentrations were then globally analyzed using a monomer-dimer equilibrium model by the SEDPHAT program (34), which gives a precise measurement for K_d (26, 35, 36).

To characterize the dimerization of BC in the presence of substrates, band-forming AUC was performed (37). Briefly, in the sample well of the double-sector band-forming centerpiece, 15 μl of wild-type BC or R16E mutant (1 mg/ml) was added before the cell was assembled. In total, 330 μl with 50 mM Hepes (pH 8.0) or with 50 mM Hepes (pH 8.0), 0.2 mM Mg-ATP, 5 mM free Mg^{2+}, 15 mM bicarbonate, and 40 mM biotin was dissolved in D_2O and loaded into the bulk sample sector space. After equilibrating to the desired temperature, the centrifuge was spun at a rotor speed of 42,000 rpm. Absorbance at 280 nm was monitored continuously using a time interval of 300 s per scan

TABLE 1
Summary of crystallographic information

Protein	Wild-type BC	Wild-type BC	R16E mutant
Ligands	2 ADP, 2 Ca^{2+}	2 ADP, Mg^{2+}	Mg-ADP, HCO$_3^-$
Space group	$C2$	$C2$	$C2$
Cell dimensions			
a, b, c (Å)	170.2, 58.8, 85.1	171.4, 58.0, 85.2	119.4, 51.2, 84.2
α, β, γ (°)	90, 94.2, 90	90, 94.6, 90	90, 119.8, 90
Resolution^a (Å)	30-2.0 (2.1-2.0)	30-1.9 (2.0-1.9)	30-2.0 (2.1-2.0)
R_{merge} (%)	10.5 (39.7)	11.7 (37.1)	7.5 (30.8)
$I/\sigma I$	10.4 (2.2)	14.9 (3.8)	10.7 (2.6)
Completeness (%)	98 (88)	99 (99)	96 (95)
Number of reflections	53,284	61,446	27,864
R factor (%)	17.0 (20.3)	20.8 (24.7)	18.0 (21.1)
Free R factor (%)	22.8 (27.5)	26.3 (32.4)	22.6 (27.1)
r.m.s. deviation in bond lengths (Å)	0.010	0.011	0.010
r.m.s. deviation in bond angles (°)	1.3	1.3	1.2

^{a} The numbers in parentheses are for the highest resolution shell.

and a step size of 0.003 cm. The scans at different time intervals were then fitted to a continuous $c(s)$ distribution model using the SEDFIT program (38, 39).

RESULTS AND DISCUSSION

Overall Structure of BC in Complex with Two ADP Molecules and Two Ca^{2+} Ions—The original goal of our experiment was to determine the binding modes of the biocytin and bicarbonate substrates to *E. coli* BC (22). We included high concentrations of both compounds (44 and 20 mM, respectively) as well as 5 mM Mg-AMPPNP in the co-crystallization conditions. Unexpectedly, based on x-ray diffraction data at 2.0 Å resolution (Table 1), we observed the binding of two ADP molecules and two Ca^{2+} ions in the active site in one of the crystals (Fig. 1*A*). The calcium ions were present in the reservoir solution, and we confirmed their identity based on the temperature factor values after crystallographic refinement. If the two cations were assumed to be Mg^{2+} ions, their *B* values were 4 and 13 Å^2, respectively, whereas the values for the two Ca^{2+} ions were 13 and 20 Å^2, comparable with that for atoms in the protein. We observed clear electron density for the two ADP molecules, with no indication for the presence of the γ-phosphate group (Fig. 1*B*). In fact, based on modeling considerations, there may be insufficient space in the structure to accommodate both γ-phosphate groups. Therefore, either AMPPNP had been partially hydrolyzed to ADP during storage and co-crystallization, or there was substantial amount of ADP in the samples of AMPPNP.

We also determined the structure of BC in complex with two ADP molecules and one Mg^{2+} ion at 1.9 Å resolution under a different crystallization condition. The crystals were prepared in the presence of Mg-ADP, and there were no Ca^{2+} ions in the reservoir.

The refined atomic models agreed well with the crystallographic data and the expected bond angles and bond lengths (Table 1). About 93% of the residues are in the most favored region of the Ramachandran plot, and none are in the disallowed region.

The two monomers of the BC dimer in the asymmetric unit have essentially the same conformation (Fig. 1*A*), with r.m.s. distances of 0.24 Å between their Cα atoms. The overall structure of the BC monomer in this complex is similar to other structures of *E. coli* BC reported earlier. For example, the r.m.s.

distance between equivalent Cα atoms of this structure and those in the structure of the complex with bicarbonate, biotin, and Mg-ADP is 0.26 Å (22). The r.m.s. distance is 0.45 Å when the structure is compared with that of the E288K mutant in complex with ATP (16). The BC dimers in the three structures are generally similar as well, with r.m.s. distances of roughly 0.7 Å. However, the position of the B domain has significant differences among these structures (see below) and is excluded from the comparisons.

Binding Modes of the Two ADP Molecules and Ca^{2+} Ions— The crystallographic analysis showed that the two ADP molecules, two Ca^{2+} ions, and associated waters have well defined electron density (Fig. 1*B*), indicating that they are ordered in the active site of BC. The first ADP molecule (named ADP1 here) occupies the position normally taken by the ATP substrate in the BC active site (16, 22), although there are also significant differences (see below). Residues Glu-201, Lys-202, and Leu-204 (in the B domain) interact with the adenine base, Gln-233 (strand β12 in the C domain) interacts with the ribose, and Lys-159 (B domain) and a Ca^{2+} ion (Ca1) interact with the α- and β-phosphates (Fig. 1*C*).

The second ADP molecule (ADP2) is placed near ADP1 in the active site of BC (Fig. 1*C*). The oxygen atom in the ribose ring of ADP2 is hydrogen-bonded to the main-chain amide of Gly-83 (in the A domain), and the N6 atom of its adenine base interacts with an oxygen atom in the side chain of Glu-87. One of the terminal oxygen atoms on the α-phosphate has ion-pair interaction with the side-chain of Arg-338 (strand β16 in the C domain). Two of the terminal oxygen atoms on the β-phosphate are recognized by bi-dentate ion-pair interactions with the side-chain guanidinium group of Arg-292 (β15-αN loop in the C domain), whereas one of them is also hydrogen-bonded to the main-chain amide of Val-295. Finally, the third terminal oxygen atom on the β-phosphate is located within 2.6 Å of the side-chain carboxylate group of Glu296 (Fig. 1*C*).

Both Ca^{2+} ions are coordinated by six ligands arranged in an octahedral fashion (Fig. 1*C*). The first Ca^{2+} ion (Ca1) is coordinated by a terminal oxygen atom from the α- and β-phosphate groups of ADP1, an oxygen atom from the side chains of Glu-276 (strand β14 in the C domain) and Glu-288 (strand β15 in the C domain), and two water molecules. The second Ca^{2+} ion (Ca2) is coordinated by an oxygen atom from the side chains of
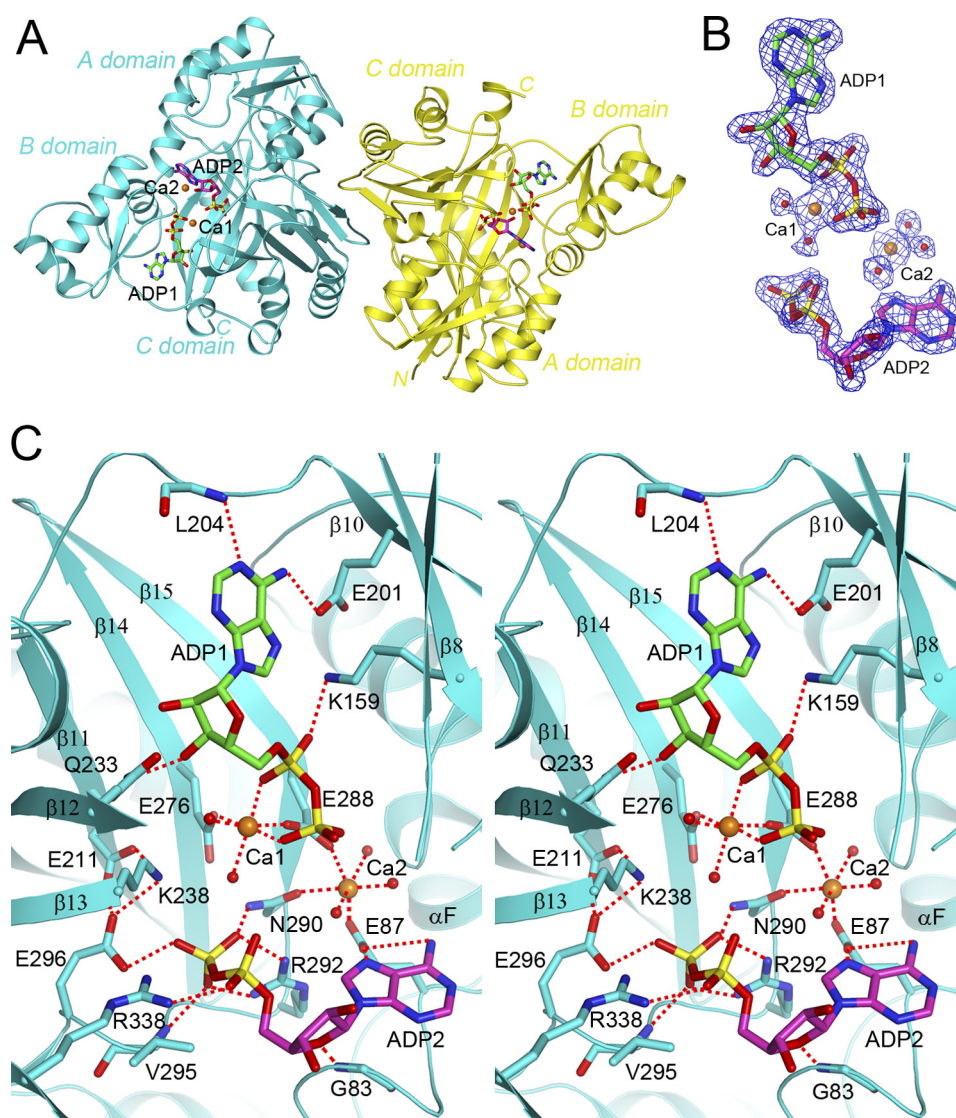
FIGURE 1. **Structure of wild-type *E. coli* BC in complex with two ADP molecules and two Ca²⁺ ions.** *A*, shown is the overall structure of the *E. coli* BC dimer in complex with ligands. The two monomers are colored in *cyan* and *yellow*, respectively. ADP1 and ADP2 are shown in *green* and *magenta* for carbon atoms, and the Ca^{2+} ions are in *orange*. *B*, final $2F_o - F_c$ electron density at 2.0 Å resolution for ADP1, ADP2, Ca1, Ca2, and associated waters (*red spheres*) contoured at 1.2σ is shown. *C*, schematic drawing in stereo shows detailed interactions in the active site of BC. Hydrogen-bonding and ion-pair interactions are indicated with the *dashed lines in red*. All structure figures were produced with PyMOL.

Glu-87 (in the A domain), Glu-288, and Asn-290 (in the $\beta15$-αN loop in the C domain) and three water molecules.

Our observations on the structure in complex with two ADPs and two Ca^{2+} ions are supported by the structure in complex with two ADPs and one Mg^{2+} ion. The two ADP molecules occupy essentially the same position in this structure, and the Mg^{2+} ion occupies the position of the first Ca^{2+} (Ca1) ion. This also confirms that the binding of ADP2 is not dependent on the presence of the second Ca^{2+} ion.

Comparison to Other BC Structures—Previous studies show that the B domain of BC can undergo large conformational changes and close over the active site upon ATP or ADP binding (16, 22). In the current structure, the B domain is placed even closer to the active site, corresponding to roughly a 14° rotation compared with the structure of BC in complex with its substrates (Fig. 2*A*) (22). Compared with the structure of the E288K mutant of BC in complex with ATP (16), a rotation of 21° in the B domain is observed (Fig. 2*B*).

The structural comparison also shows that ADP2 occupies the positions of the bicarbonate and biotin substrates of BC (Figs. 2, *C* and *D*). The ribose and the α-phosphate of ADP2 overlap with the ureido ring of biotin. Especially, one of the terminal oxygen atoms on the α-phosphate is in the same position as the ureido oxygen and maintains the same interaction with the Arg-338 side chain (Fig. 2*C*), consistent with earlier suggestion that Arg-338 helps stabilize the biotin enolate during catalysis (22). The β-phosphate has very good overlap with the bicarbonate substrate (Fig. 2*D*) and is recognized in a similar fashion, especially the interactions with the side chains of Arg-292 and Glu-296 (Fig. 2*C*).

The further closure of the B domain in the current structure is coupled with a movement in the bound position of ADP1 as compared with the earlier structures (Fig. 2*C*). The $C\alpha$ atom of Lys-159 moves by 3.7 Å as compared with that in the structure of the complex with all substrates (22), and the bound position of ADP1 is shifted by 1.7 Å (Fig. 2*C*). With
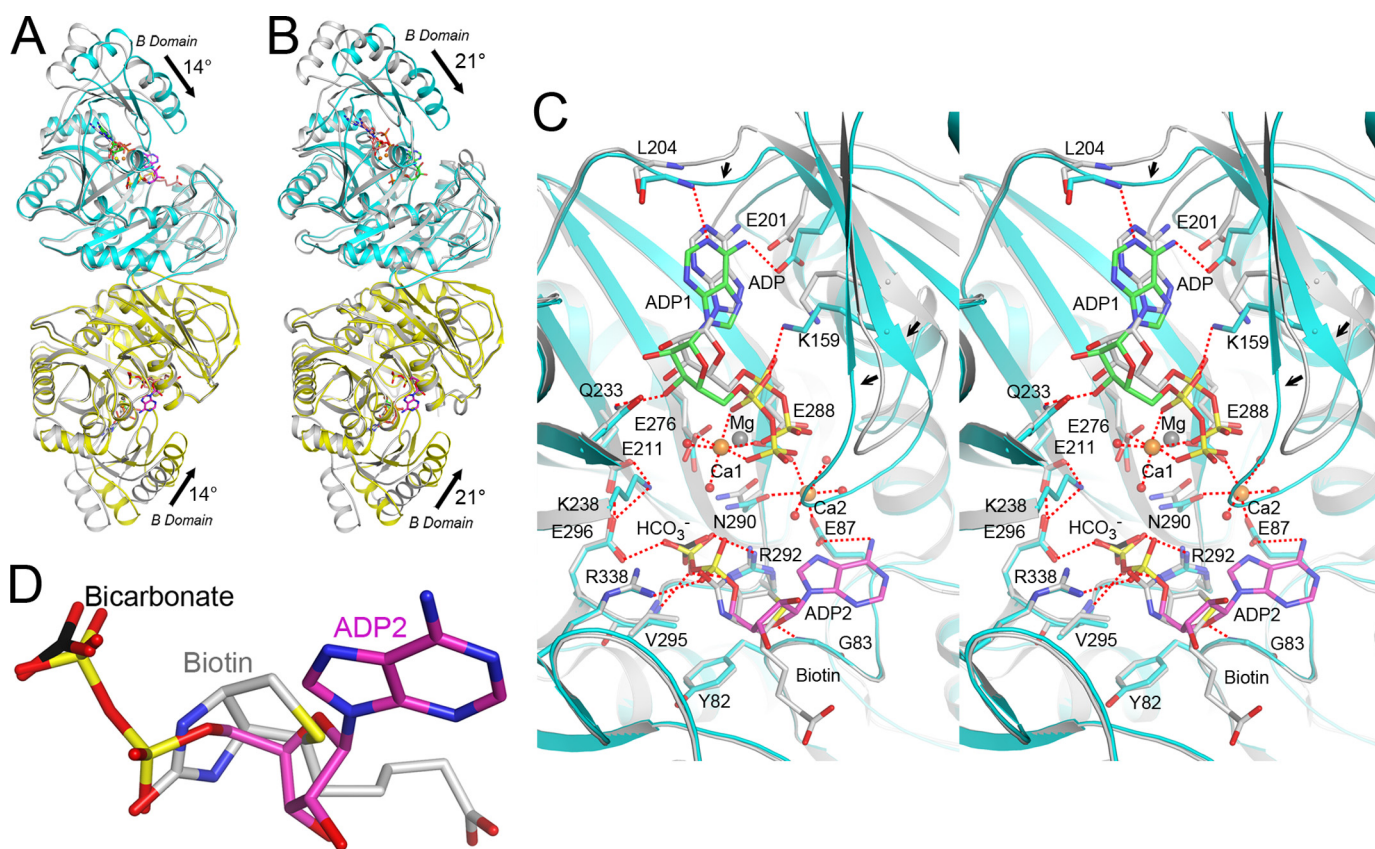
FIGURE 2. **Comparisons with other structures of BC.** *A*, shown is overlay of the current structure of *E. coli* BC dimer (in *cyan* and *yellow*) in complex with two ADPs and two Ca^{2+} ions with that of BC dimer (*gray*) in complex with all substrates (22). The conformational difference of domain B is indicated with the *arrows*. *B*, overlay of the current structure of *E. coli* BC dimer (in *cyan* and *yellow*) with that of E288K mutant BC dimer (*gray*) in complex with ATP (16) is shown. A larger conformational difference of domain B is observed. *C*, overlay of the active site region comparing the binding modes of the two ADP molecules and two Ca^{2+} ions with those of bicarbonate (*black*), biotin (*gray*), ADP (*gray*), and Mg^{2+} (*yellow*) (22) is shown. The *small arrows* indicate the change in the conformation of the B domain. *D*, shown is a close-up showing the overlay of ADP2 with bicarbonate and biotin.

this further closure of the B domain, the binding site for ADP2 (and, hence, biotin and bicarbonate) is also more buried, suggesting that this conformation may be more relevant catalytically. The electron density for the B domain in the current structure is stronger than that in the complex with all substrates (22), indicating that the B domain may be stabilized upon the binding of ADP2.

In the structure of *Staphylococcus aureus*, BC bound to AMPPNP and two Mg^{2+} ions (23), one of the Mg^{2+} ions is located between the α- and γ-phosphates and is about 1.3 Å away from Ca1 of the current structure. The other Mg^{2+} ion is located between the β- and γ-phosphates and is 1.9 Å away from Ca2. However, Ca2 can only interact with the γ-phosphate and is too far from the β-phosphate. Therefore, the binding mode of Ca2 is quite different from that of the second Mg^{2+} ion in this earlier structure.

Kinetic Studies Confirm Substrate Inhibition by ATP, Competitive Versus Bicarbonate—The location of ADP2 in the binding sites for bicarbonate and biotin suggests that ADP (and ATP) may inhibit the catalytic activity of BC. Indeed, our kinetic data showed a non-hyperbolic pattern at higher Mg-ATP concentrations (Fig. 3*A*). Based on fitting to the substrate inhibition model (Equation 1), the K_i for ATP is about 27 mM, whereas the apparent K_m and k_{cat} values are similar to those reported earlier (Table 2) (26). These

studies indicate that the ATP substrate can inhibit BC catalysis at high concentrations, confirming our structural observations.

To characterize the pattern of inhibition between ATP and bicarbonate, we carried out kinetic assays with bicarbonate as the substrate and at varying concentrations of Mg-ATP. The observed kinetic parameters showed an increase in the apparent K_m for bicarbonate at increasing Mg-ATP concentrations, whereas the k_{cat} was not affected significantly (Table 3). This is clearly indicative of a competitive pattern of inhibition *versus* bicarbonate, consistent with our structural observations. The analysis of the kinetic data was complicated by the fact that Mg-ATP is also a substrate of the enzyme, and therefore, the classical competitive inhibition equation may not be completely appropriate for these data. In addition, there was endogenous bicarbonate in the buffers that was not removed before the assays. The current analysis assumed 1.5 mM endogenous bicarbonate in the buffers, which gave the lowest errors for the kinetic parameters. The estimated K_i value for ATP ranges between 2 and 6 mM for endogenous bicarbonate concentrations between 1 and 8 mM. Overall, data from the bicarbonate competition assays (Table 3) and the ATP substrate inhibition assay (Fig. 3*A*) suggest that the K_i for ATP is in the 5–20 mM range.

We tested whether other nucleotides also have an inhibitory activity on BC catalysis. Mg-GTP, Mg-CTP, and Mg-TTP showed similar inhibitory activity against BC (Fig. 3*B*). Al-
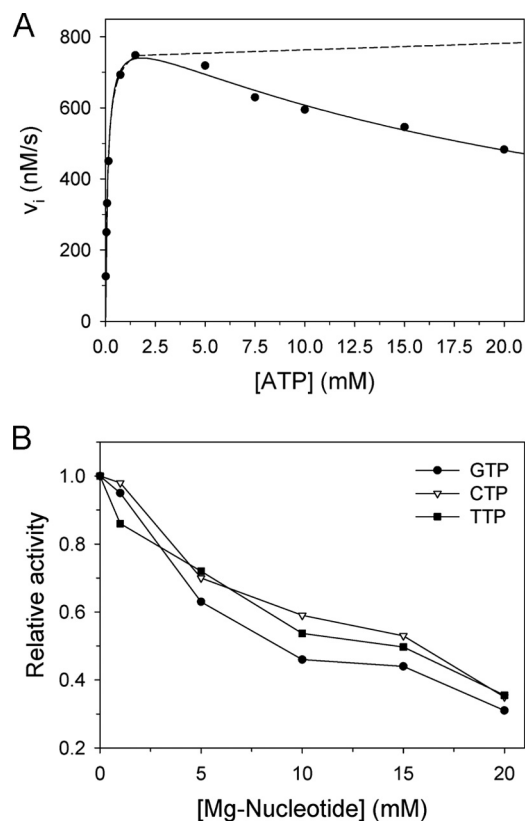
FIGURE 3. **Initial velocity patterns of *E. coli* BC and inhibition by nucleotides.** *A*, shown is a plot of the initial velocity of BC at various ATP concentrations. The *dashed* and *solid lines* represent the results fitted according to the Michaelis-Menten equation and substrate-inhibition equation (Equation 1), respectively. *B*, a plot shows the inhibition of the activity of *E. coli* BC by various concentrations of GTP (*circles*), CTP (*open triangles*), and TTP (*squares*), respectively. The reaction mixture contained 0.2 mM ATP and 5 mM free Mg^{2+}.

TABLE 2

Summary of kinetic parameters for wild-type BC and R16E mutant
ND, not done.

Protein[a]	Apparent $K_{m,ATP}$	Apparent k_{cat}	$k_{cat}/K_{m,ATP}$	$K_{i,ATP}$
	mM	s^{-1}	s^{-1} mM^{-1}	mM
wt BC	0.12 ± 0.01	0.36 ± 0.01	3000 ± 179	27.0 ± 2.0
R16E	0.12 ± 0.01	0.20 ± 0.01	1667 ± 162	ND

[a] The values for wild-type BC (wt BC) were from the best fit to substrate inhibition model (Equation 1), whereas those for R16E were from the Michaelis-Menten equation. After best fitting, R_{sqr} of wt BC and R16E was 0.996 and 0.998, respectively. All assays were repeated several times to ensure reproducibility.

TABLE 3

ATP shows a competitive pattern of inhibition against bicarbonate

Mg-ATP concentration	Apparent K_{m,HCO_3^-}[a]	Apparent k_{cat}	$k_{cat}/K_{m,HCO_3^-}$
mM	mM	s^{-1}	s^{-1} mM^{-1}
1.5	1.9 ± 0.3	0.31 ± 0.01	162 ± 22
7.5	5.0 ± 1.5	0.36 ± 0.06	71 ± 16
10	6.5 ± 0.7	0.32 ± 0.01	49 ± 4
20	11.4 ± 2.6	0.30 ± 0.03	26 ± 4

[a] The endogenous bicarbonate concentration in the buffers was assumed to be 1.5 mM in the assays, which produced the lowest errors for the kinetic parameters. Fitting the observed data to the competitive model of inhibition gave 1.3 ± 0.4 mM for K_{m,HCO_3^-}, 0.32 ± 0.01 s^{-1} for k_{cat}, and 2.6 ± 1.0 mM for K_i of Mg-ATP. Varying the endogenous bicarbonate concentration from 1 to 8 mM changed the K_i from 2 to 6 mM.

though we cannot exclude the possibility that these nucleotides compete against the natural ATP substrate, it is likely that they inhibit by binding in the ADP2 site. The adenine base in the

ADP1 site is recognized by several hydrogen-bonding interactions, whereas the adenine base in the ADP2 site has fewer interactions with the enzyme (Fig. 1*C*). Therefore, the ADP2 site may have lower selectivity among the different nucleotides. In addition, the inhibitory activity of these other nucleotides is similar to that of Mg-ATP, with apparent IC$_{50}$ values of about 10 mM (Fig. 3*B*), consistent with the hypothesis that they function through the ADP2 site. We were not able to check the inhibition by ADP, GDP, and CDP, as the coupling enzyme (pyruvate kinase) in the assay can immediately convert them to the triphosphate form.

The structure also suggests that pyrophosphate may be inhibitory, by competing against biotin and bicarbonate (Fig. 2*D*). Our kinetic results confirmed that magnesium pyrophosphate could inhibit BC, although with lower potency (20% inhibition at 5 mM concentration) compared with the nucleotides. Inhibitory activity at higher concentrations of pyrophosphate could not be tested due to rapid precipitation of the compound in the presence of Mg^{2+}. Pyrophosphate is known to be a potent product inhibitor of *E. coli* biotin protein ligase (BirA) (40, 41), which attaches the biotin group to biotin carboxyl carrier protein. Our studies demonstrate that pyrophosphate may also regulate BC catalysis, in addition to its other important roles in cellular biochemistry (42).

Characterization of the Monomer-Dimer Equilibrium of the R16E Mutant—Previously we introduced mutations in the dimer interface of *E. coli* BC that disrupted interactions between the monomers and found that the R19E and E23R mutations greatly reduced the stability of the dimer (26). Arg-19 and Glu-23 (both in helix αA) have ion-pair interactions with Glu-408′ and Arg-401′ (both in helix αO′) in the dimer interface, respectively (the *primed residue numbers* indicate the other monomer) (Fig. 4). In the current study we introduced another mutation near the dimer interface, R16E. This residue (also in helix αA) does not directly contact the other monomer but is involved in ion-pair interactions with Glu-301 (in helix αL) and Asp-307 (in the αL-αM loop). These two residues contribute to the binding site of Phe-363′ (Fig. 4), which makes the largest contribution to the buried surface area in the dimer interface (26).

We characterized the monomer-dimer equilibrium of the R16E mutant by AUC experiments. The data showed that the mutation greatly reduced the stability of the dimer, and the K_d value of 445 ± 43 μM for this mutant is actually similar to those of the R19E and E23R mutants that we studied earlier (26). Therefore, the Arg-16 residue also has an important role in dimer formation of *E. coli* BC, even though it is not directly in the dimer interface.

To further characterize the monomer-dimer equilibrium of the R16E mutant, we used the band-forming AUC technique to examine if there is substrate-induced dimerization (Fig. 5*A*). The size distributions showed that wild-type BC is dimeric (3.9 Svedberg) in the absence or presence of substrates (Fig. 5*B*). In comparison, the R16E mutant was monomeric (2.7 S) in the absence of substrates, whereas it contained 78% monomer and 22% dimer in the presence of substrates (0.2 mM Mg-ATP, 5 mM free Mg^{2+}, 15 mM bicar-
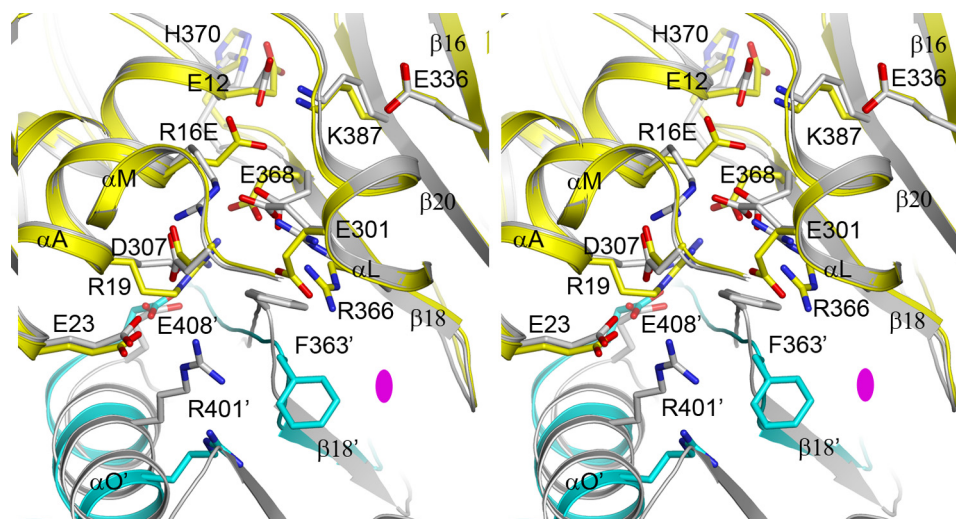
FIGURE 4. Dimer interface of *E. coli* BC. Overlay of the dimer interface of R16E mutant (in *yellow* and *cyan* for the two monomers) with that of wild-type BC (in *gray*). The monomer in *yellow* is superimposed onto the wild-type structure, and a large change in the monomer in *cyan* is visible. Side chains with important roles in the dimer interface are shown as *stick models*. The 2-fold axis of the dimer is indicated with the *magenta oval*.
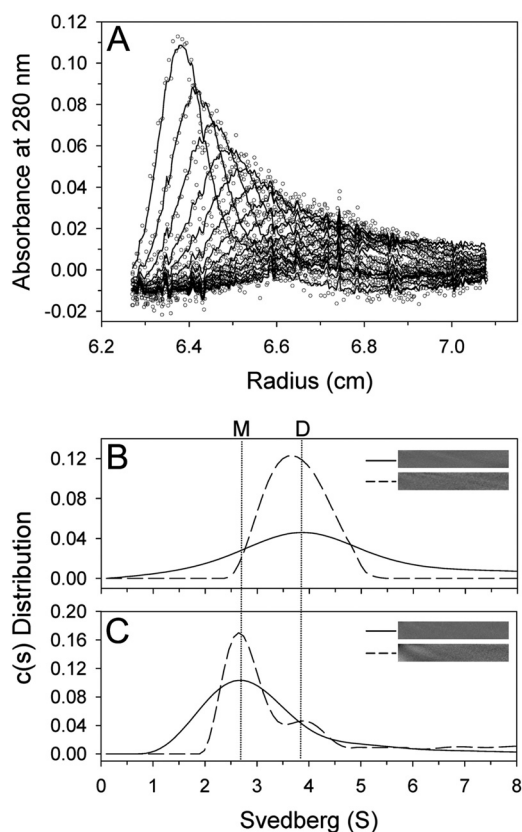
FIGURE 5. Band-forming AUC pattern of wild-type BC and R16E mutant. *A*, shown is a typical trace of absorbance at 280 nm of the wild-type BC during the experiment. *Symbols* represent experimental data, and *lines* are the results fitted to the Lamm equation using the SEDFIT program (37, 39). *B* and *C*, continuous *c(s)* distributions of wild-type BC and R16E mutant from the best-fit analysis, respectively, are shown. The residual bitmaps of the raw data and the best-fit results are shown in the *insets*. The protein amount used is 15 μl (1 mg/ml), and the total volume of the cell is 330 μl. The distributions in 50 mM Hepes (pH 8.0) are shown by *solid lines*, and those in substrate mixture are shown by *dashed lines*. The *dotted line* on the *left* indicates monomer (*M*), and the *one on the right* indicated dimer (*D*) position.

bonate, and 40 mM biotin) (Fig. 5*C*). This substrate-induced dimerization phenomenon has also been observed in coronavirus main protease (37).

Our kinetic studies showed that the R16E mutant had only a 2-fold loss in catalytic activity compared with the wild-type enzyme (Table 2). This activity cannot be completely explained by the 22% dimeric species that is induced by the substrates. Therefore, the data suggest that monomeric R16E mutant is active as well, consistent with our earlier studies on the R19E and E23R mutants (26).

Crystal Structure of R16E Mutant in Complex with Mg-ADP and Bicarbonate—We next determined the crystal structure of the R16E mutant at 2.0 Å resolution (Table 1). In the co-crystallization experiment, 20 mM bicarbonate, 44 mM biocytin, and 5 mM Mg-ATP were included in the protein solution. The crystallographic analysis revealed the binding of Mg-ADP and bicarbonate in the active site. The overall structure of the R16E monomer is similar to that of wild-type BC in complex with all substrates (Fig. 6*A*) (22), with an r.m.s. distance of 0.6 Å. Three neighboring β-strands, β17, β19, and β21, show recognizable structural differences (Fig. 6*A*) due to the re-organization of the dimer interface (see below).

In the active site region, there are only a few conformational changes. Bicarbonate and Mg-ADP have essentially the same binding modes as those to the wild-type enzyme (Fig. 6*B*). The β16-β17 loop (residues 340–352) has a different conformation and would clash with the binding of biotin (Fig. 6*B*). This conformation appears to be unique to this crystal form of the R16E mutant and is not observed in other structures of *E. coli* BC. This loop is involved in crystal packing in the R16E mutant structure, and therefore, the observed conformation may be stabilized by crystal packing and may not be a direct consequence of the R16E mutation. The conformation of this loop may be more flexible in solution, consistent with the data that this mutant has only a 2-fold loss in activity compared with the wild-type enzyme (Table 2). The structure of this loop may also be associated with the conformational change for strand β17 in the R16E mutant (Fig. 6*A*).

Large Re-organization of the Dimer in the R16E Mutant—There is a monomer of the R16E mutant in the asymmetric unit of the crystal. A dimer of the mutant can be generated with the
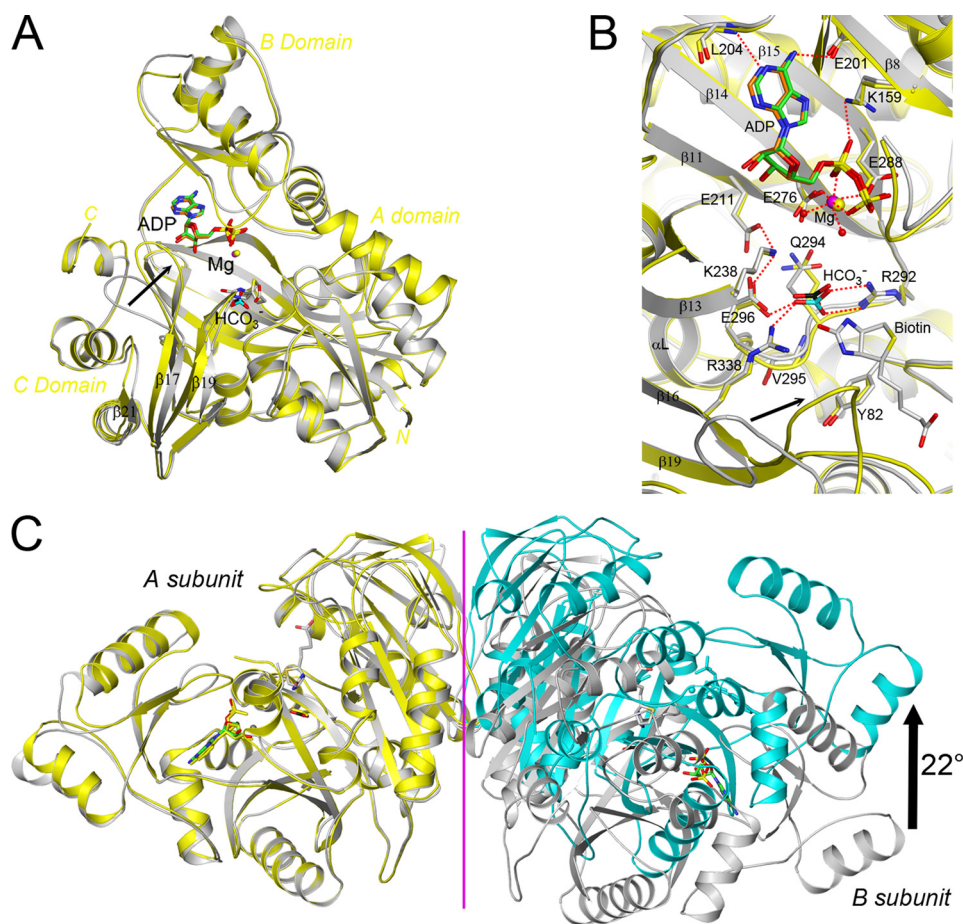
FIGURE 6. **Structure of the R16E mutant of *E. coli* BC in complex with ligands.** *A*, shown is an overlay of the structure of R16E mutant monomer (in *yellow*) in complex with bicarbonate (*cyan*) and Mg-ADP (*magenta-orange*) with that of the wild-type BC (in *gray*) with all substrates (22). The *black arrow* indicates the movement of the β16-β17 loop. *B*, shown is an overlay of the active site region of BC, comparing the binding modes bicarbonate and Mg-ADP in the R16E mutant with those of all substrates in wild-type BC (22). The *black arrow* indicates the movement of the β16-β17 loop. *C*, shown is an overlay of the R16E mutant dimer (in *yellow* and *cyan*) with that of wild-type dimer with all substrates (in *gray*). The *yellow monomer* is superimposed with the wild-type structure, and the *black arrow* indicates the large change in the orientation of the *cyan monomer*. The 2-fold axis of the dimer is indicated with the *magenta line*.

crystallographic 2-fold symmetry axis. Approximately 1100 Å² of the surface area of each monomer is buried in the interface of this dimer, which is comparable with the 1300 Å² buried surface area for the wild-type BC dimer (26). Other packing contacts in the R16E mutant crystal have much smaller buried surface areas, between 300 and 600 Å². The observation of this dimer is consistent with the high concentrations of the mutant that are present in the crystallization solution as well as our data showing substrate-induced dimerization for this mutant. In addition, our earlier studies of the R19E and E23R mutants also showed dimeric enzymes in the crystal, even though they are monomeric in solution and have similar K_d values as the R16E mutant (26). The physiological relevance of the dimer form of the R16E mutant remains to be established.

The R16E mutation did cause a large change in the organization of the BC dimer. As expected, the mutation disrupted the ionic interactions with Glu-301 and Asp-307. The side chain of R16E points in the opposite direction as compared with that of Arg-16 and interacts with the side chain of Lys-387 (strand β21) (Fig. 4). Lys-387 has ionic interactions with the side chains of Glu-12 and Glu-336 in the wild-type enzyme. In the R16E mutant, the side chain of Glu-12 points in the opposite direc-

tion and interacts with His370 instead (Fig. 4). The new position of the R16E side chain also caused a large change in the side-chain conformation of Glu-368.

With the loss of ion-pair interactions with Arg-16, a conformational change was observed for the side chain of Glu-301, and consequently its other interaction partner Arg-366 (strand β19) (Fig. 4). The new position of the Glu-301—Arg-366 ion pair, especially that of Glu-301, clashes with the position of Phe-363′. This may have triggered the large re-organization of the dimer interface. The change in this interface also breaks the Glu-23—Arg-401′ ion pair that is observed in the wild-type dimer (Fig. 4).

Another indication of the large re-organization of the dimer interface is the change in the relative orientations of the two monomers. If one monomer of the R16E dimer is superimposed with that of the wild-type dimer, the other monomers of the two dimers differ by a 22° rotation (Fig. 6C). This re-organization is much larger than that observed earlier for the E23R mutant, where the two monomers differ only by 3.5° in orientation (26). Crystal packing differences between the wild-type enzyme and the R16E mutant may have contributed to some extent to the observed change in

dimer organization, although it is unlikely that this change is due solely to crystal packing.

The B domain of the R16E mutant structure is more open compared with the structure in complex with two ADP molecules, with a 10° rotation. The conformation of this domain is actually more similar to that of the complex with all substrates, with a 5° rotation.

Our studies have identified two more substrate binding modes of *E. coli* BC. One is the binding of two ADPs and one or two metal ions and the other is that of bicarbonate and Mg-ADP. These binding modes together with those on the binding of ATP and of all substrates (bicarbonate, biotin, and Mg-ADP) reported earlier (16, 22, 23) have implications for understanding BC. During BC catalysis, it is believed that binding of bicarbonate and Mg-ATP is random and that biotin can only bind to the enzyme-bicarbonate-Mg-ATP complex (21). Our studies on the R16E mutant have revealed the conformation of the bicarbonate-Mg-ADP complex of BC, whereas our studies on the wild-type enzyme here suggest an updated scheme for BC catalysis, which allows the binding of two ATPs. The binding of the second ATP molecule (or ADP, other nucleotides, pyrophosphate) is inhibitory and is competitive against bicarbonate and most likely biotin as well.

The physiological effect of BC inhibition by ATP and other nucleotides remains to be demonstrated. Although the K_i for ATP appears to be fairly high (5–20 mM), there is no strong selectivity toward the base of the nucleotides. Therefore, BC may be sensitive to the total concentration of the NTPs (and possibly NDPs) in the cell. It might be possible that these compounds together can regulate BC activity under certain physiological conditions.

REFERENCES

1. Guchhait, R. B., Polakis, S. E., Dimroth, P., Stoll, E., Moss, J., and Lane, M. D. (1974) *J. Biol. Chem.* **249,** 6633–6645
2. Waldrop, G. L., Rayment, I., and Holden, H. M. (1994) *Biochemistry* **33,** 10249–10256
3. Tong, L. (2005) *Cell. Mol. Life Sci.* **62,** 1784–1803
4. Knowles, J. R. (1989) *Annu. Rev. Biochem.* **58,** 195–221
5. Zhang, H., Yang, Z., Shen, Y., and Tong, L. (2003) *Science* **299,** 2064–2067
6. Huang, C. S., Sadre-Bazzaz, K., Shen, Y., Deng, B., Zhou, Z. H., and Tong, L. (2010) *Nature* **466,** 1001–1005
7. Xiang, S., and Tong, L. (2008) *Nat. Struct. Mol. Biol.* **15,** 295–302
8. St Maurice, M., Reinhardt, L., Surinya, K. H., Attwood, P. V., Wallace, J. C., Cleland, W. W., and Rayment, I. (2007) *Science* **317,** 1076–1079
9. Kanamori, T., Kanou, N., Atomi, H., and Imanaka, T. (2004) *J. Bacteriol.* **186,** 2532–2539
10. Sloane, V., and Waldrop, G. L. (2004) *J. Biol. Chem.* **279,** 15772–15778
11. Höschle, B., Gnau, V., and Jendrossek, D. (2005) *Microbiology* **151,** 3649–3656
12. Jiang, H., Rao, K. S., Yee, V. C., and Kraus, J. P. (2005) *J. Biol. Chem.* **280,** 27719–27727
13. Blanchard, C. Z., Lee, Y. M., Frantom, P. A., and Waldrop, G. L. (1999) *Biochemistry* **38,** 3393–3400
14. Shen, Y., Volrath, S. L., Weatherly, S. C., Elich, T. D., and Tong, L. (2004) *Mol. Cell* **16,** 881–891
15. Sloane, V., Blanchard, C. Z., Guillot, F., and Waldrop, G. L. (2001) *J. Biol. Chem.* **276,** 24991–24996
16. Thoden, J. B., Blanchard, C. Z., Holden, H. M., and Waldrop, G. L. (2000) *J. Biol. Chem.* **275,** 16183–16190
17. Kondo, S., Nakajima, Y., Sugio, S., Yong-Biao, J., Sueda, S., and Kondo, H. (2004) *Acta Crystallogr. D Biol. Crystallogr.* **60,** 486–492
18. Kondo, S., Nakajima, Y., Sugio, S., Sueda, S., Islam, M. N., and Kondo, H. (2007) *Acta Crystallogr. D Biol. Crystallogr.* **63,** 885–890
19. Cho, Y. S., Lee, J. I., Shin, D., Kim, H. T., Cheon, Y. H., Seo, C. I., Kim, Y. E., Hyun, Y. L., Lee, Y. S., Sugiyama, K., Park, S. Y., Ro, S., Cho, J. M., Lee, T. G., and Heo, Y. S. (2008) *Proteins* **70,** 268–272
20. Cho, Y. S., Lee, J. I., Shin, D., Kim, H. T., Jung, H. Y., Lee, T. G., Kang, L. W., Ahn, Y. J., Cho, H. S., and Heo, Y. S. (2010) *Biochem. Biophys. Res. Commun.* **391,** 187–192
21. Tipton, P. A., and Cleland, W. W. (1988) *Biochemistry* **27,** 4317–4325
22. Chou, C. Y., Yu, L. P., and Tong, L. (2009) *J. Biol. Chem.* **284,** 11690–11697
23. Mochalkin, I., Miller, J. R., Evdokimov, A., Lightle, S., Yan, C., Stover, C. K., and Waldrop, G. L. (2008) *Protein Sci.* **17,** 1706–1718
24. Janiyani, K., Bordelon, T., Waldrop, G. L., and Cronan, J. E., Jr. (2001) *J. Biol. Chem.* **276,** 29864–29870
25. Weatherly, S. C., Volrath, S. L., and Elich, T. D. (2004) *Biochem. J.* **380,** 105–110
26. Shen, Y., Chou, C. Y., Chang, G. G., and Tong, L. (2006) *Mol. Cell* **22,** 807–818
27. Yu, L. P., Xiang, S., Lasso, G., Gil, D., Valle, M., and Tong, L. (2009) *Structure* **17,** 823–832
28. Otwinowski, Z., and Minor, W. (1997) *Methods Enzymol.* **276,** 307–326
29. McCoy, A. J., Grosse-Kunstleve, R. W., Adams, P. D., Winn, M. D., Storoni, L. C., and Read, R. J. (2007) *J. Appl. Crystallogr.* **40,** 658–674
30. Jones, T. A., Zou, J. Y., Cowan, S. W., and Kjeldgaard, M. (1991) *Acta Crystallogr. A* **47,** 110–119
31. Brünger, A. T., Adams, P. D., Clore, G. M., DeLano, W. L., Gros, P., Grosse-Kunstleve, R. W., Jiang, J. S., Kuszewski, J., Nilges, M., Pannu, N. S., Read, R. J., Rice, L. M., Simonson, T., and Warren, G. L. (1998) *Acta Crystallogr. D Biol. Crystallogr.* **54,** 905–921
32. Murshudov, G. N., Vagin, A. A., and Dodson, E. J. (1997) *Acta Crystallogr. D Biol. Crystallogr.* **53,** 240–255
33. Hsu, W. C., Chang, H. C., Chou, C. Y., Tsai, P. J., Lin, P. I., and Chang, G. G. (2005) *J. Biol. Chem.* **280,** 22741–22748
34. Schuck, P. (2003) *Anal. Biochem.* **320,** 104–124
35. Lin, P. Y., Chou, C. Y., Chang, H. C., Hsu, W. C., and Chang, G. G. (2008) *Arch. Biochem. Biophys.* **472,** 34–42
36. Bai, Y., Auperin, T. C., Chou, C. Y., Chang, G. G., Manley, J. L., and Tong, L. (2007) *Mol. Cell* **25,** 863–875
37. Chou, C. Y., Hsieh, Y. H., and Chang, G. G. (2011) *Methods* **54,** 76–82
38. Brown, P. H., and Schuck, P. (2006) *Biophys. J.* **90,** 4651–4661
39. Schuck, P. (2000) *Biophys. J.* **78,** 1606–1619
40. Ng, B., Polyak, S. W., Bird, D., Bailey, L., Wallace, J. C., and Booker, G. W. (2008) *Anal. Biochem.* **376,** 131–136
41. Kukko, E., and Heinonen, J. (1982) *Eur. J. Biochem.* **127,** 347–349
42. Ho, A. M., Johnson, M. D., and Kingsley, D. M. (2000) *Science* **289,** 265–270